Journal of Applied Biomechanics, 2020, 36, 249-258
https://doi.org/10.1123/jab.2019-0088

Human Kinetics
COMPUTATIONAL MODEL

Sensitivity of Neuromechanical Predictions to Choice of Glenohumeral Stability Modeling Approach

Daniel C. McFarland, Alexander G. Brynildsen, and Katherine R. Saul
North Carolina State University

Most upper-extremity musculoskeletal models represent the glenohumeral joint with an inherently stable ball-and-socket, but the physiological joint requires active muscle coordination for stability. The authors evaluated sensitivity of common predicted outcomes (instability, net glenohumeral reaction force, and rotator cuff activations) to different implementations of active stabilizing mechanisms (constraining net joint reaction direction and incorporating normalized surface electromyography [EMG]). Both EMG and reaction force constraints successfully reduced joint instability. For flexion, incorporating any normalized surface EMG data reduced predicted instability by 54.8%, whereas incorporating any force constraint reduced predicted instability by 43.1%. Other outcomes were sensitive to EMG constraints, but not to force constraints. For flexion, incorporating normalized surface EMG data increased predicted magnitudes of joint reaction force and rotator cuff activations by 28.7% and 88.4%, respectively. Force constraints had no influence on these predicted outcomes for all tasks evaluated. More restrictive EMG constraints also tended to overconstrain the model, making it challenging to accurately track input kinematics. Therefore, force constraints may be a more robust choice when representing stability.

Keywords: EMG, shoulder, computational modeling, joint reaction, simulation

In vivo glenohumeral joint motion involves not only rotation, but also translation[1]; modeling this mobile joint is challenging. Many musculoskeletal models neglect translation, representing the joint as a ball-and-socket.[2–4] This assumption makes the modeled joint inherently stable; however, stabilization in vivo is provided through coordinated cocontraction of surrounding muscles to balance net glenoid joint reaction force (JRF).[5] Inherent stability of a ball-and-socket presents a challenge when using optimization to solve for muscle activations because cost functions typically minimize muscular effort.[6] Solutions with cocontractions are typically avoided as they increase muscular effort without contributing to resulting motion. Consequently, cocontractions necessary for joint stability may be neglected, resulting in poor predicted outcomes for JRF,[7] rotator cuff forces, and instability metrics. To ameliorate this, researchers have proposed methods to incorporate cocontraction into optimization; 2 common approaches are constraining predicted muscle excitations to match magnitudes of normalized surface electromyography (EMG) signals within a tolerance[8] or constraining optimization to direct JRF within the glenoid.[2,3,9] Constraining predicted muscle excitations to normalized surface EMG signals may either constrain on/off timing or the entire signal within a tolerance.[8] Nikooyan et al,[8] however, showed that model predictions depended on how many muscles were constrained, with high numbers overconstraining the model and leading to poor predictions. Force constraints instead address the balance of glenohumeral JRF rather than muscle coordination, using one of 2 mechanisms by which JRFs are stabilized in vivo: concavity compression and scapulohumeral balance.[5] Concavity compression (pressing the humeral head into the glenoid)[3,9,10] constrains shear to compressive force ratio to fall within multidirection dislocation force ratios determined through cadaveric studies.[11,12] Scapulohumeral balance requires the JRF to pass through the glenoid to maintain humeral head balance.[2,13]

Although effects of both EMG and force constraints have been individually evaluated, analyses are typically made on only one predicted outcome. For example, Dickerson et al[3] evaluated effects of concavity compression constraints on predicted muscle forces, but not on glenohumeral reaction forces; Nikooyan et al[8] evaluated effects of ±5% EMG tolerance on predicted JRFs, but not on predicted muscle forces. Furthermore, although Nikooyan et al[8] incorporates both EMG and force constraints, interactions of these constraints were not evaluated. Direct comparison of techniques to model stabilizing forces in inherently stable glenohumeral joints for multiple outcomes would provide a valuable foundation for appropriate model decision making.

Our goal is to present and compare predictions of simulated outputs using common types of stability constraints and characterize sensitivity of these results. Specifically, we evaluate sensitivity of 3 predicted outcomes (instability, glenohumeral JRF, and rotator cuff activations) to modeling choices for incorporating stability (EMG constraints and force constraints). Our hypotheses were that inclusion of any stability constraints (force or EMG) would lower predicted instability and influence timing and magnitude of JRFs and rotator cuff activation curves, but constraint style would not influence predictions.

Methods

Musculoskeletal Modeling

Simulations were performed in OpenSim (version 3.3; Stanford, CA)[14] with a previously developed and validated upper-extremity musculoskeletal model[15] representing a 50th percentile male. Shoulder rotations are defined using International Society of Biomechanics standards,[16] with constrained scapulohumeral

The authors are with the Department of Mechanical and Aerospace Engineering, North Carolina State University, Raleigh, NC, USA. Saul (ksaul@ncsu.edu) is corresponding author.

rhythm.[17] Muscle–tendon units representing muscles crossing the glenohumeral (15 actuators) and elbow (10 actuators) joints were included, implemented using Millard muscle models[18] with force–length, force–velocity, and tendon curves adjusted to reflect relationships described by Binder-Markey and Murray.[19] For each subject, the model was scaled to anthropometry using a static motion capture trial.

Computational Simulations

We performed computed muscle control (CMC) simulations[20,21]—augmented to include glenohumeral stability constraints—of abduction and forward flexion (details on data collection used to inform simulations are presented in following subsections). A total of 15 CMC simulations per task per subject (5 EMG and 3 force conditions and interactions) were performed. In total, we simulated 4 subjects during 2 tasks for a total of 120 simulations. In brief, the CMC algorithm incorporates error dynamics to determine joint accelerations required to track experimental kinematics, a static optimization to calculate required muscle activations to produce desired joint accelerations, and an excitation controller to drive a forward dynamic simulation which creates simulated joint kinematics that feedback into the error dynamics. Full details of the CMC algorithm have been previously reported.[20,21]

Simulation Constraints

Altogether, we evaluate 2 styles of EMG constraints at 3 levels of muscles constrained (all, subset, and none) for a total of 5 EMG conditions per subject per task. The 2 styles of incorporating normalized surface EMG signals into the CMC optimization were constraining (1) on/off timing of excitations and (2) simulated excitations within ±5% of normalized surface EMG signals.[8] For the on/off timing constraint, the muscle was considered off when normalized EMG signal was <0.1; calculated excitation was limited to 0.1. Otherwise, the muscle was considered on; calculated excitation was required to exceed 0.1. Both timing and tolerance constraints were applied by adjusting upper and lower bounds between which a specific muscle's activations must lie. Nikooyan et al[8] compared EMG-driven simulations against experimentally determined JRF and reported better tracking when only a subset of recorded muscles was incorporated. Therefore, our simulations were performed with constraints applied to both the entire set of recorded muscles and a subset; we used optimal subsets reported by Nikooyan et al.[8] For abduction, the subset included sternal pectoralis major and triceps long head. For forward flexion, the subset included all deltoid components, clavicular pectoralis major, and brachioradialis.

We evaluated 2 methods of controlling JRF direction within the glenoid: concavity compression[3,9] and scapulohumeral balance[2,13] in addition to simulations where JRF direction was not constrained. For constrained simulations, CMC optimization was augmented with a penalty term to encourage resultant JRF (calculated using OpenSim joint analysis tool[22]) toward stability limits and prevent theoretical glenohumeral subluxation. For concavity compression, JRF was decomposed into compressive and shear forces; the shear to compressive force ratio was constrained to fall within empirical stability limits from cadaveric studies.[5,11] These stability limits were determined in multiple directions (eg, anterior–posterior, superior–inferior) by compressing the humeral head into the glenoid and determining the shear force required for joint dislocation. Here, concavity compression stability limits (shear to compressive force ratios) were derived from Halder et al,[11] who reported average stability ratios measured at 4 levels of shoulder abduction and 3 force levels. For scapulohumeral balance constraint, JRF was constrained to remain within the glenoid ellipse boundary[2] derived from experimental measurements.[5] For both styles of JRF constraint, a penalty term proportional to the extent to which JRF exceeds the stability criterion was applied to the optimization:

$$J = \sum_{i=1}^{n} x_i^2 + \sum_{j=1}^{m} \ddot{q}_j^{*} - \ddot{q}_j^{\,2} + p \cdot (\text{S–L})|_{S>L} \quad (1)$$

where p is a constant scaling the penalty term. For concavity compression, S is shear force and L is allowed shear determined from compressive force and empirical stability ratios.[11] For scapulohumeral balance, S is radial distance of JRF projected onto the glenoid and L is radial distance of glenoid boundary defined by an ellipse. The penalty term was applied if $S > L$. The default CMC function used in simulations without force constraints is the same as above without the additional penalty term.

A sensitivity analysis on the effect of constant p was performed. For this analysis, only force constraints were applied and p was varied from 0 to 0.25; resulting peak instability, JRF, and rotator cuff activations were plotted against p. This sensitivity analysis was performed for abduction task for the 4 subjects because abduction had an unstable JRF over a longer range of thoracohumeral elevation when neither EMG nor force constraints were applied, compared with the flexion task. Based on the sensitivity analysis, p was set to .05 for remaining simulations.

Experimental Data Collection

Kinematic and EMG data were simultaneously collected for 4 subjects (participant details presented below) to inform computational simulations. Kinematic data were collected using 7 motion capture cameras (Motion Analysis Corp, Santa Rosa, CA) tracking sixteen 1-cm retroreflective markers placed on anatomical landmarks (Figure 1).[23] Prior to testing, a static trial in which all markers were visible to cameras was collected for scaling. Kinematic motion capture data were postprocessed and smoothed with a 6-Hz Butterworth filter. Anthropometrically scaled models were used to obtain joint angle trajectories for each task through inverse kinematics. Resultant joint kinematics were filtered with a zero-phase filter in MATLAB (The MathWorks, Natick, MA).

Unilateral surface EMG recordings of anterior, middle, and posterior deltoid; biceps brachii; triceps brachii long head; latissimus dorsi; clavicular and sternal components of pectoralis major; and brachioradialis were collected (Figure 1). Recordings were made at 2000 Hz using 1-cm Ag/AgCl dual electrodes (Noraxon, Scottsdale, AZ). Electrodes were placed on skin overlying the muscle belly following recommendations of Cram and Criswell.[24] Prior to testing, subjects performed maximum voluntary contractions (MVCs) against manual resistance following a standard protocol[25]; the MVC test for biceps brachii was also applied for brachioradialis. Exertions were obtained over 5 seconds; each muscle was tested 3 times with 2 minutes of rest between trials. EMG data for each task were normalized using the maximum value for each muscle from any MVC trial.[26]

Testing Protocol

Subjects performed 3 trials each of unweighted abduction and forward flexion trials, with 30-second rest between trials; task order was randomized. Subjects were instructed to abduct or forward flex

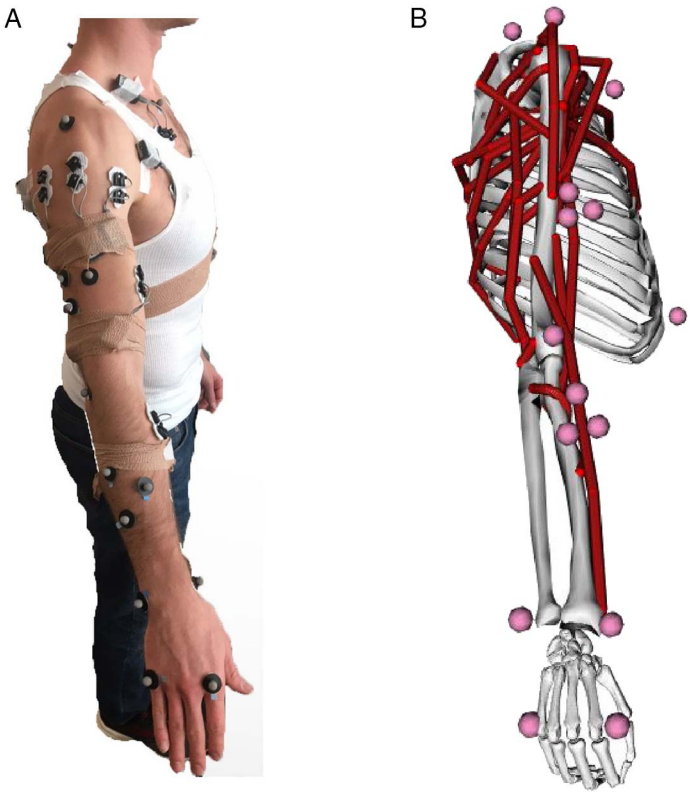

Figure 1 — (A) Experimental setup included 9 electromyography electrodes and 16 retroreflective markers. (B) Musculoskeletal model used in the simulation with 25 muscle–tendon units crossing the glenohumeral and elbow joints. Virtual markers on the models are displayed in spheres.

to the end of their range of motion at a rate of 2 seconds per movement. The second trial of each task for each participant was postprocessed to obtain input kinematics and normalized EMG signals for computational simulation.

Participants

Four healthy young adults (2 males and 2 females) aged 20–25 years participated. On average, participants were 22.5 (2.9) years old, 170.4 (9.2) cm, and 77.1 (5.2) kg. Participants met inclusion criteria: (1) no history of upper limb injury, (2) no neuromuscular impairments, and (3) no physical impediment to performing exertions. All subjects were self-reported right-dominant; the dominant hand was used. All subjects provided written informed consent in accordance with North Carolina State University Institutional Review Board. Each subject completed the protocol in 1 session.

Statistical Analysis

For each simulated task, we evaluated the effect of simulation constraints on predicted instability, calculated JRF normalized to bodyweight, and calculated rotator cuff activations. Predicted instability is calculated as a percentage of empirical stability limit determined from cadaveric studies[11]:

$$\frac{\left(\text{Shear force}/\text{Compressive force}\right)}{\left(\text{Empirical stability limit}\right)} \times 100 \qquad (2)$$

where glenohumeral JRF is decomposed into shear and compressive components, and the empirical stability limit is defined according to shear component direction. We also calculate predicted instability using the scapulohumeral balance constraint in the denominator (Figure 2) to demonstrate that both calculations result in stable JRF at approximately the same thoracohumeral elevation; thus, only the empirical stability limit was used for remaining analyses. For predicted peak instability, peak JRF, and peak sum of rotator cuff activations (supraspinatus, subscapularis, and infraspinatus), a 2-way analysis of variance ($\alpha < .05$; factors: EMG and force constraints) was performed. For predicted instability, when interactions were not present, they were removed from the model and Tukey honest significant difference post hoc test was performed; when interaction was present, a simple main effects test was performed with a 1-way analysis of variance at each factor level of the interaction. For JRF and rotator cuff activations, if an interaction was present, data were grouped by each level of interaction for subsequent analysis; otherwise data were grouped by single factor (EMG or force constraints). Statistical parametric mapping (SPM) *t* tests[27,28] were used to determine differences from default condition (no EMG and no force constraint) in postural dependence of outcome over thoracohumeral elevation. Due to the exploratory nature of the study, we did not adjust α for multiple comparisons.

Results

This work evaluated sensitivity of predicted outcomes (instability, glenohumeral JRF, and rotator cuff activations) to modeling choices for incorporating stability (EMG constraints and force constraints). Most simulations ran successfully, although the more restrictive EMG tolerance constraint required higher reserve actuators to successfully track experimental kinematics. Reserve actuators were included to provide additional joint torque where required to track kinematics.[29] Mean root mean squared reserve torque was <1.0 N·m for all coordinates for all trials; simulations requiring reserve torque >5 N·m are reported (Table 1). Of the 120 simulations, 3 simulations (2.5%) failed to converge during optimization and were removed from analysis. Converged simulations had mean root mean squared error between input and CMC kinematics <1.1° and maximum tracking error <5° for every degree of freedom. Subjects performed tasks at a consistent speed; task duration was 0.67 (0.12) seconds (0.50–0.87 s) for 30° to 90° thoracohumeral elevation.

Sensitivity analysis of penalty constant p revealed that the value of p had little impact on instability and other outcomes. Including a penalty term lowered instability; however, larger values of p did not further lower instability. Larger p caused some simulations to fail to converge (Supplementary Figure 1 [available online]).

Inclusion of EMG or force constraints lowered predicted instability. When no constraints were applied, instability reached or exceeded empirical limits in low thoracohumeral elevations (Figure 2) for both tasks. When applied, EMG and force constraints were main effects on predicted instability ($P < .001$); interactions between force and EMG constraints were significant for flexion ($P < .001$), but not for abduction ($P = .22$). For flexion with no force constraints, applying any EMG constraint significantly lowered predicted instability to within empirical limits ($P < .001$; Figure 3) when compared with no EMG constraint, by 54.8% on average. Likewise, for flexion, with no EMG constraints, applying any force constraint significantly lowered predicted instability ($P < .001$)

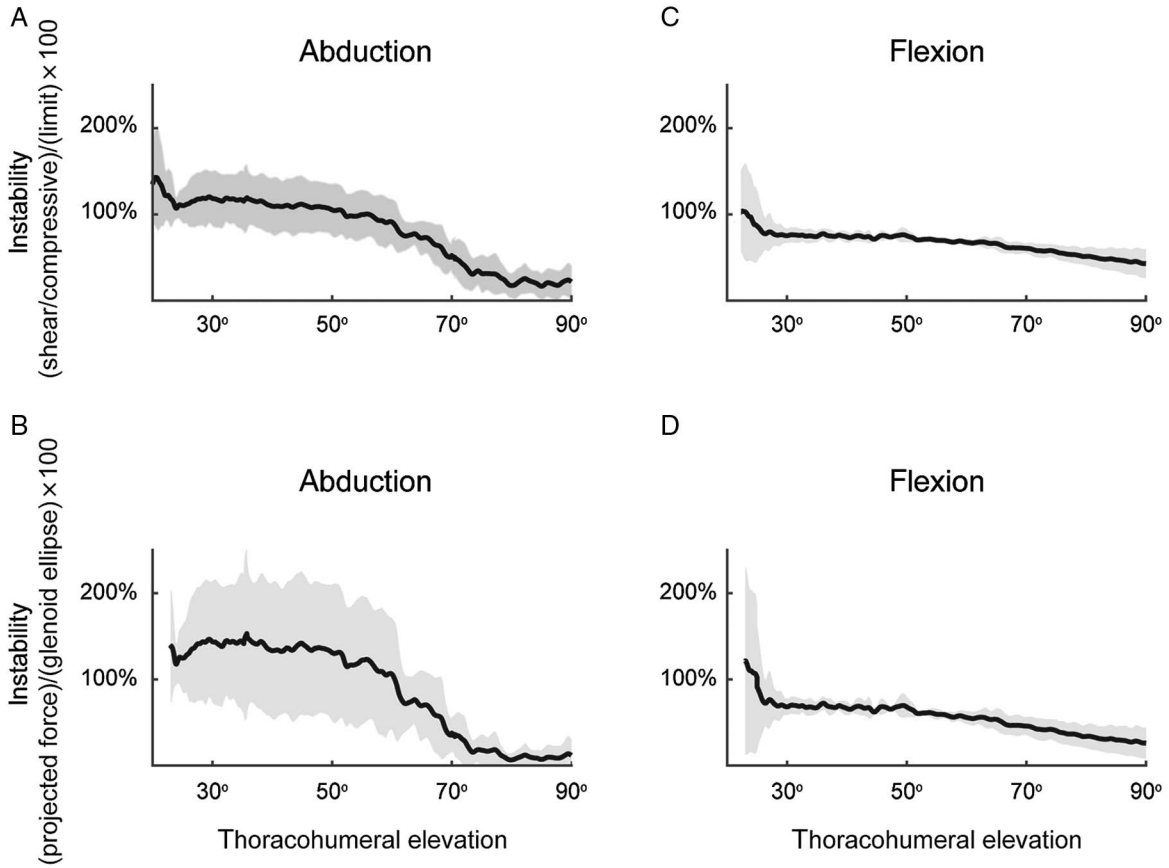

Figure 2 — Glenohumeral instability during abduction (left) and flexion (right). (A) Glenohumeral instability defined according to the limits of the concavity compression constraint (empirical stability limit). (B) Glenohumeral instability defined according to the limits of the scapulohumeral balance constraint. Predicted instability (mean: black line; 1 SD: shaded) of the subjects when neither force nor electromyography constraints were applied reached or exceeded empirical stability limits (100%) primarily in low thoracohumeral elevations.

Table 1 Simulations With High Reserve Torques

Removed task	Subject	Force constraint	Electromyography constraint	Reserve (N)
Abduction	Male subject 1	Scapulohumeral balance	Tolerance all	6.0
			Tolerance subset	6.0
		Concavity compression	Tolerance all	6.2
			Tolerance subset	6.3
		None	Tolerance all	6.0
			Tolerance subset	5.7
	Female subject 1	Scapulohumeral balance	Tolerance all	7.4
		Concavity compression	Tolerance all	7.4
		None	Tolerance all	7.3

when compared with no force constraint by 43.1% on average. Although predicted instability was lowered when any force constraint was applied to the no EMG condition, instability remained slightly above empirical stability limits (<104% of the limit). In contrast, for flexion, using any EMG constraint with a force constraint lowered predicted instability to within empirical stability limits; whether this reduction was significant depended on the interaction between constraints (Figure 3). For abduction, post hoc analysis revealed including either force constraint significantly lowered instability ($P < .01$; Figure 4), by 22.5% on average. For abduction, including the full set of muscles with either EMG constraint significantly reduced instability compared with no EMG ($P < .05$) by 36.2% on average. Using the muscle subset with either EMG constraint did not significantly lower predicted instability compared with no EMG for abduction ($P = .95$).

Inclusion of EMG constraints had substantial influence on predicted JRF, whereas force constraints resulted in nonsignificant JRF differences of <100 N (Figure 5). EMG constraints were

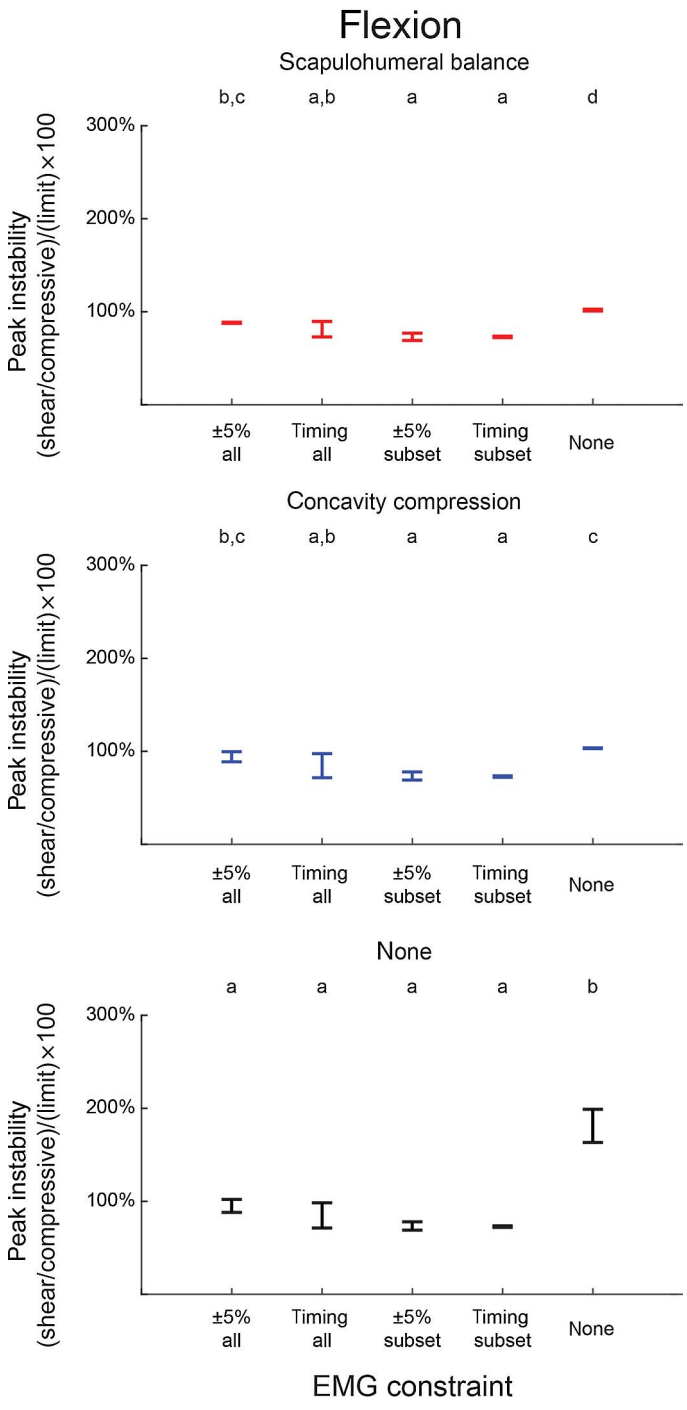

Figure 3 — Interaction plot of electromyography and force constraints on peak glenohumeral instability during flexion. Mean peak predicted instability (percentage of empirical stability limit) for scapulohumeral balance (top), concavity compression (middle), and no force constraint (bottom) are plotted against the 5 electromyography constraint styles. Significant differences among electromyography conditions when considering only one force constraint condition (ie, scapulohumeral balance, concavity compression, and none) are denoted above the individual panels with letters. If letters are different from each other, there is a significant difference between electromyography constraint styles. For example, none condition is significantly different from all other conditions when no force constraint is applied (bottom panel). The only significant differences among force conditions for a given electromyography condition were for the none electromyography condition.

present as main effects ($P < .05$), but force constraints and interactions were not ($P > .9$). Post hoc analysis revealed that constraining the full set of muscles with ±5% tolerance resulted in higher peak JRF than other conditions ($P < .05$). For abduction, this most constrained condition resulted in higher peak JRF than simulations with tolerance constraint applied only to the muscle subset (increased 27.3%). For flexion, this most constrained condition resulted in higher peak JRF than simulations without EMG constraints (increased 37.2%). For both tasks, the type of EMG constraint impacted overall postural dependence. For abduction, SPM analysis revealed higher JRFs at low thoracohumeral elevation postures when either EMG constraint was applied to the entire set of recorded muscles; both subset EMG constraints were not different from the none condition. The region over which significant differences were detected was smaller for on/off timing compared with ±5% tolerance. For flexion, SPM analysis revealed significantly higher JRF at low thoracohumeral elevation when any EMG data were used a constraint. EMG constraint style and number of muscles included had minor impact.

Inclusion of EMG constraints on surface muscles has a significant influence on predicted rotator cuff activations; however, inclusion of force constraints caused only subtle but nonsignificant increases at low elevations where reaction forces were near empirical stability limits. EMG constraints were present as main effects ($P < .0001$), but force constraints were not ($P = .99$). Post hoc analysis revealed that for both tasks, inclusion of EMG constraints increased predicted rotator cuff activations. For flexion, including any EMG constraint resulted in significantly higher peak activations than for no EMG constraint ($P < .001$; increased 88.4% on average; Figure 6). Furthermore, SPM analysis of postural dependence revealed that including any normalized EMG resulted in significantly higher rotator cuff activations throughout the range of motion for flexion. For abduction, including all surface muscles for either EMG constraint style resulted in higher peak activation than including the subset or no EMG ($P < .001$; increased 23.8% on average; Figure 7). For abduction, the number of muscles included was more influential than constraint style; only simulations that included all recorded muscles significantly increased activations. For these abduction simulations, SPM analysis revealed a slight difference between constraint styles only if all recorded muscles were constrained; under this condition, the stricter ±5% tolerance influenced rotator cuff activations throughout a larger range of elevation postures than timing constraint.

Discussion

We evaluated effects of force and EMG constraints on predicted glenohumeral instability, net glenohumeral JRF, and rotator cuff activations during abduction and forward flexion. Without stability constraints, instability was at or over empirical limits at low thoracohumeral elevations, consistent with the observation that outcomes were most sensitive to including stability constraints in these postures. Predicted instability was influenced by both EMG and force constraints, whereas net JRF and rotator cuff activations were influenced by inclusion of normalized surface EMG data, but not force constraints.

Predicted instability results suggest that either constraining direction of glenohumeral JRF or constraining muscle excitation patterns to normalized surface EMG signals can be appropriate methods of incorporating stability. Both force constraints stabilized reaction forces; for flexion, when no EMG data were included, predicted instability was still slightly over empirical limits. This,

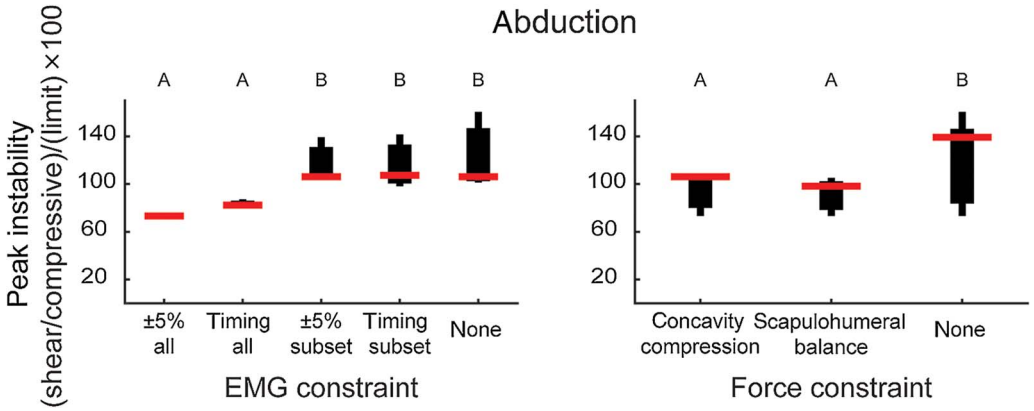

Figure 4 — Effect of electromyography (left) and force (right) constraints on peak glenohumeral instability during abduction. Main effects of each electromyography and force constraint on mean peak predicted instability (percentage of empirical stability limit) during abduction. Differences in predicted instability among constraints are denoted with letters.

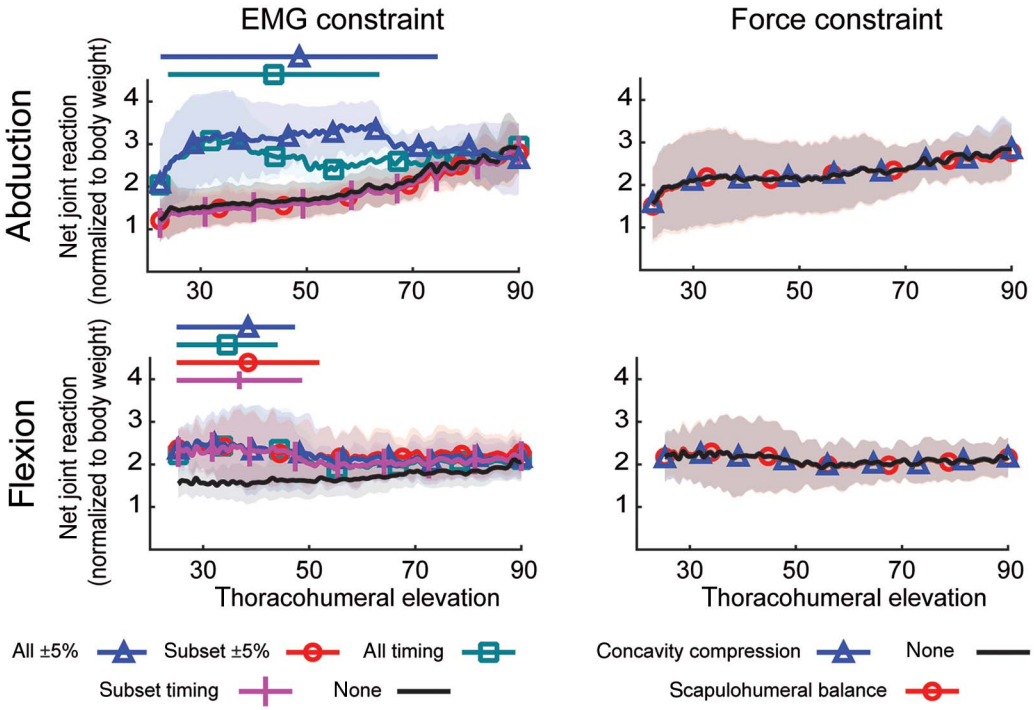

Figure 5 — Net glenohumeral JRF normalized by bodyweight for abduction (top) and flexion (bottom). Because there was no interaction between EMG (left) and force (right) constraints for JRF, reaction forces are grouped by constraint type. Bars above the plots denote regions over which predicted JRF differ as compared with the no constraint condition, as determined by SPM. EMG indicates electromyography; JRF, joint reaction force; SPM, statistical parametric mapping.

however, is likely acceptable because stability limits vary based on posture,[11] and some humeral head translation occurs in vivo.[1] Using EMG was appropriate for incorporating stability if enough muscles were included. For flexion, the subset of muscles was appropriate to stabilize the glenohumeral joint. For abduction, all recorded muscles had to be included to stabilize the joint. Therefore, muscle selection should be carefully considered when using EMG to enforce glenohumeral stability. One reason EMG constraints were more successful at stabilizing the glenohumeral joint using the flexion subset compared with the abduction subset is that the flexion subset included all deltoid compartments, whereas the abduction subset did not. Incorporating both EMG and force constraints is likely unnecessary because either alone significantly reduces predicted instability.

Predicted glenohumeral JRF and rotator cuff activations were only sensitive to inclusion of normalized surface EMG. While we do not have an instrumented endoprosthesis or indwelling fine-wire EMG recordings for rotator cuff muscles here, and thus cannot evaluate accuracy for these specific participants, we contextualize predicted outcomes against relevant literature. Including EMG

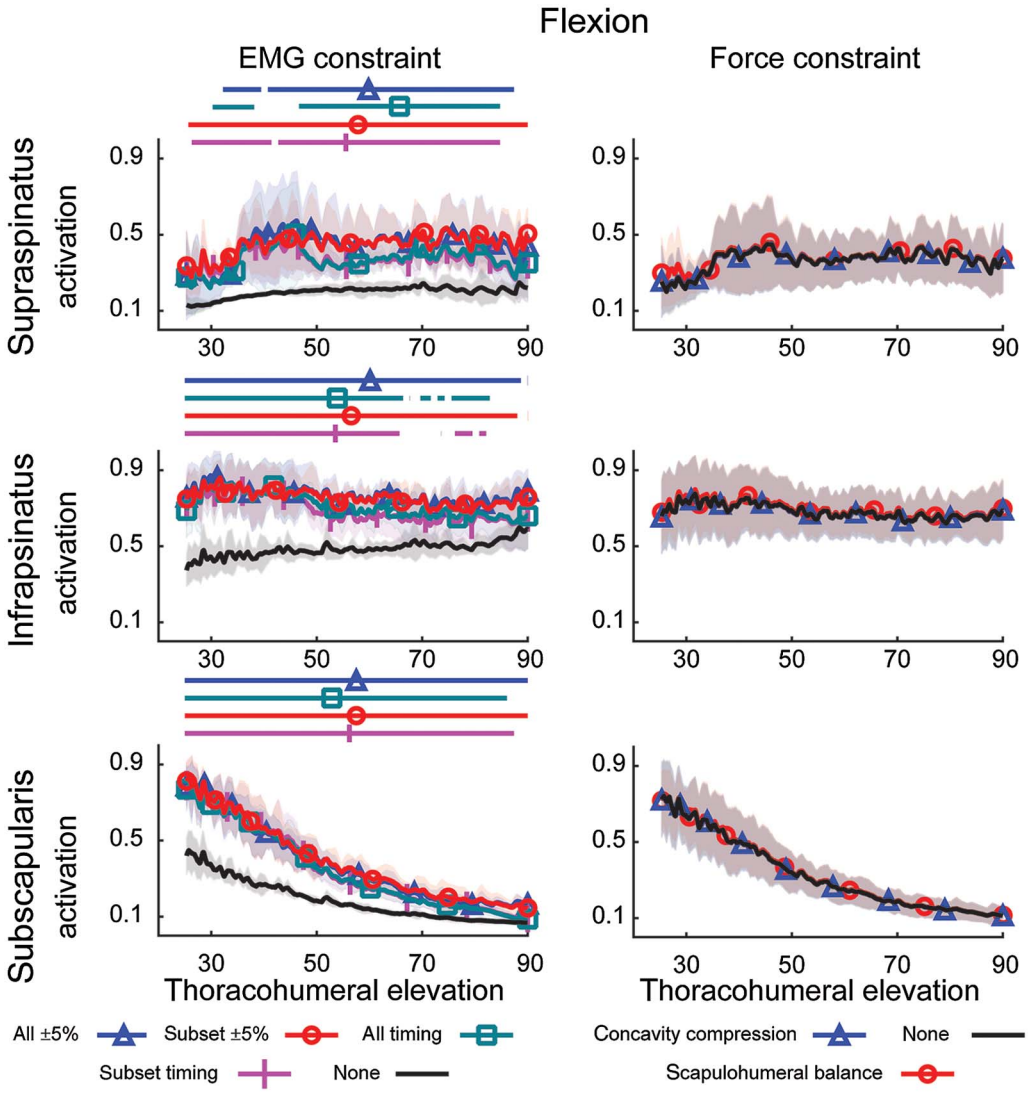

Figure 6 — Effects of EMG (left) and force (right) constraints on predicted rotator cuff activations for supraspinatus (top), infraspinatus (middle), and subscapularis (bottom) during flexion. Bars above the plots denote regions over which predicted rotator cuff activations differ as compared with the no constraint condition, as determined by SPM. EMG indicates electromyography; SPM, statistical parametric mapping.

constraints did not improve consistency with previously reported glenohumeral JRF[7,8] or rotator cuff EMG signals.[30,31] For example, in the current work using the full set of recorded muscles resulted in high JRF at low thoracohumeral elevations for both abduction and flexion; experimental results suggest a gradual increase in JRF.[7,8] Peak JRF measured with an instrumented endoprosthesis have been reported up to 1.2 × bodyweight for unweighted flexion and abduction[7,32,33] and up to 2.38 × body weight for low-weighted forward flexion.[34] Other in vivo studies report JRF up to 1.7 × body weight for various tasks.[32,33,35] Our predicted JRFs are consistent with or slightly higher than these values when no EMG constraints are applied, ranging 1.2 to 2.9 times body weight. Previous studies that calculate glenohumeral JRF forces with a computational model for various upper-extremity tasks have also reported peak JRF between 1.3 and 2.7.[34,35] However, when more restrictive EMG constraints were applied to our tasks, predicted JRF reached 3.4 × body weight, exceeding reported literature values, likely due to becoming overconstrained.[8] Thus, our results suggest that using a large set of EMG signals as constraints may not improve JRF predictions.

It should be noted that in vivo measurements of JRF require instrumented endoprosthesis, limiting use to individuals experiencing osteoarthritis who are typically older and often have rotator cuff damage. As a result, these subjects can have difficulty in performing tasks that are relatively easy for healthy young adults. For example, Bergmann et al[34] report that some subjects were unable to abduct or forward flex with a 2-kg weight. In the Nikooyan et al[7] study, subjects were instructed to elevate to the maximal angle possible which ranged from 80° to 120°. This suggests that there are differences in capacity compared with healthy young adult subjects, which may manifest in JRF. Therefore, it is not possible to confirm our simulation results against experimental in vivo JRF of healthy adults.

Using surface muscle, EMG constraints also caused predicted rotator cuff activations that were not fully consistent with reported fine wire EMG recordings from rotator cuff. For example, Heuberer et al[30] report low subscapularis and infraspinatus EMG signals throughout flexion and abduction, while inclusion of EMG constraints increased predicted activations for these muscles.

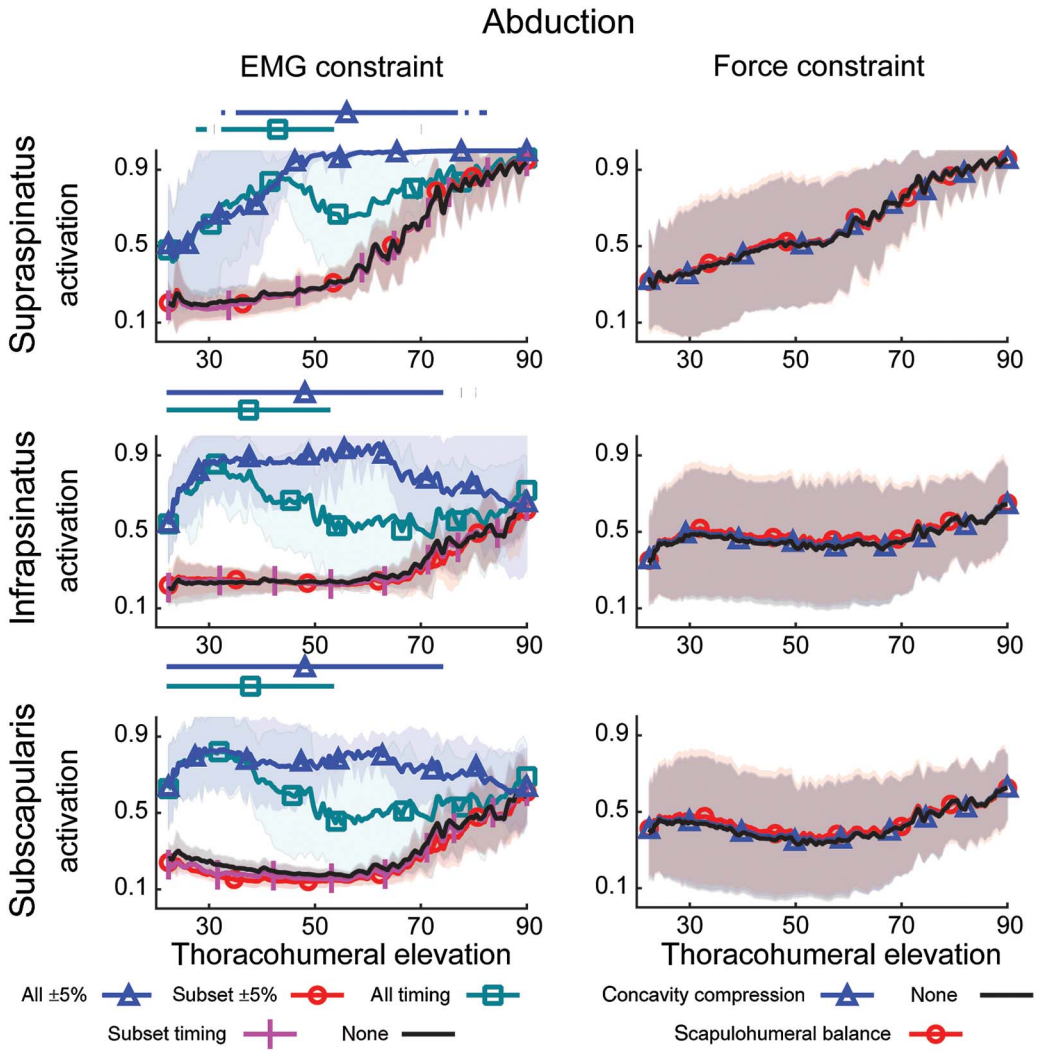

Figure 7 — Effects of EMG (left) and force (right) constraints on predicted rotator cuff activations for supraspinatus (top), infraspinatus (middle), and subscapularis (bottom) during abduction. Bars above the plots denote regions over which predicted rotator cuff activations differ as compared with the no constraint condition, as determined by SPM. EMG indicates electromyography; SPM, statistical parametric mapping.

For flexion, even EMG constraints applied to the muscle subset caused high rotator cuff activations throughout the motion, possibly because this subset of muscles included all deltoid components. For abduction, EMG constraints applied to the muscle subset (which did not include deltoid) did not cause a significant change from no EMG condition. Thus, choice of muscles to constrain is critical, as it significantly affects sensitivity of all 3 predicted outcomes considered here.

EMG-based stability constraints may fail to improve predicted outcomes for several reasons, including issues inherent to EMG and modeling simplifications. Signal noise (cross talk, movement artifacts, and so on), time delays, and normalization challenges all introduce error to EMG signal that may confound application as direct controls within a modeling framework. For example, several studies have reported difficulty capturing true peaks for normalization of dynamic tasks during standardized isometric MVC activities.[8,36–38] In addition, modeling simplifications may contribute to errors in predicted outcomes when using EMG as controls. Many upper-extremity simulation studies do not account for strength differences between individual subjects and the default model[7,8,39–41]; differences in strength between a model and subjects could result in different shoulder dynamics for a given EMG control set. Furthermore, musculoskeletal models inherently represent the musculoskeletal system with reduced complexity. For example, a volumetric muscle may be represented with limited muscle paths, and application of limited EMG signals to these actuators can overconstrain the simulation solution. Prior work by Quental et al[42] concluded that, in general, greater muscle discretization leads to better prediction of muscle forces. However, Nikooyan et al,[8] using the Delft Shoulder and Elbow Model with 139 muscle elements, still found that using all recorded normalized EMG signals as constraints caused simulation failure. Therefore, careful consideration of which surface muscles to constrain is needed. Nikooyan et al[8] suggest that constraining only one cocontracting muscle may be appropriate, and muscle choice should depend on task similarity to forward flexion or abduction. In the current study, constraining 2 muscles to normalized surface EMG signals for abduction did not significantly alter JRF or rotator cuff activations compared with including no EMG, suggesting that limiting muscle selection may avoid

overconstraining but provide limited value. This is in line with findings of Nikooyan et al[8] who reported that while incorporating EMG data could sometimes improve predicted JRF; importantly, some EMG-constraint conditions in their study caused worse predictions or simulation failure. If EMG constraints are incorporated, on/off timing may be more appropriate, as output sensitivity was lower compared with ±5% tolerance and avoids some concerns related to EMG normalization.

Including force constraints had no significant influence on peak JRF magnitude or rotator cuff activations. Our findings are consistent with Blache et al,[9] who compared concavity compression with no constraint and reported minor changes in magnitude of shear and compressive forces between conditions, suggesting a tradeoff of shear for compressive forces to enforce stability without marked change in JRF magnitude. Several studies have reported sensitivity of predicted muscular effort to force constraints[9,40,41]; these differing reports may be related to a difference in empirical stability limits employed. Empirical stability limits vary across studies,[5,11] with other models using limits either more conservative[3,9] or less conservative than those used here.[2] Dickerson et al[3] reported increased muscle forces with more conservative limits when they evaluated a range of limits. While we did not explore differing empirical stability limits here, we did evaluate sensitivity to the magnitude of the penalty constant and found no improvement in predicted stability with increased penalty.

Study limitations should be considered when interpreting these results. Experimental glenohumeral reaction forces and rotator cuff EMG signals were not measured for our subjects; therefore, our analysis is limited to sensitivity of simulation outputs to simulation constraints. We evaluated simulation sensitivity for abduction and forward flexion between 20° and 90°; however, sensitivity of predicted outcomes to evaluated constraints may differ for other functional tasks or postures. We used inputs from 4 healthy young adult subjects to drive simulations; sensitivity to constraints may vary for other populations, for example, subjects with rotator cuff injury.

In summary, predicted instability was successfully controlled by both force and EMG constraints; however, EMG constraints' ability to control predicted instability depended on choice of muscles. Peaks and postural dependence of JRF and predicted rotator cuff activations were more sensitive to including normalized EMG data than force constraints. More restrictive EMG constraints tended to overconstrain the model, resulting in higher reserve torques, and when contextualized with reported experimental outcomes, may not necessarily improve predictions. Furthermore, using larger muscle sets for EMG constraints resulted in more variability from the default unconstrained condition in all predicted outcomes. As a result, an EMG timing constraint with fewer included muscles may be more appropriate than a tolerance constraint; it is less likely to overconstrain and depends less on normalization. However, careful consideration of which muscles to include to ensure the constraint enforces stability, but does not overconstrain the model. On the other hand, force constraints improved predicted instability but had no influence on peak value or postural dependence for JRF or rotator cuff activations. Force constraint style had little impact on outcomes. Therefore, force constraints may be more appropriate when just glenohumeral stability is considered.

Acknowledgment

The authors have no conflicts of interest to disclose.

References

1. Cereatti A, Calderone M, Buckland DM, Buettner A, Della Croce U, Rosso C. In vivo glenohumeral translation under anterior loading in an open-MRI set-up. *J Biomech*. 2014;47(15):3771–3775. PubMed ID: 25307436 doi:10.1016/j.jbiomech.2014.09.021
2. Chadwick EK, Blana D, van den Bogert A J, Kirsch RF. A real-time, 3-D musculoskeletal model for dynamic simulation of arm movements. *IEEE Trans Biomed Eng*. 2009;56(4):941–948. PubMed ID: 19272926 doi:10.1109/TBME.2008.2005946
3. Dickerson CR, Chaffin DB, Hughes RE. A mathematical musculoskeletal shoulder model for proactive ergonomic analysis. *Comput Methods Biomech Biomed Engin*. 2007;10(6):389–400. PubMed ID: 17891574 doi:10.1080/10255840701592727
4. Holzbaur KR, Murray WM, Delp SL. A model of the upper extremity for simulating musculoskeletal surgery and analyzing neuromuscular control. *Ann Biomed Eng*. 2005;33(6):829–840. PubMed ID: 16078622.
5. Lippitt SB, Matsen F. Mechanisms of glenohumeral joint stability. *Clin Orthop Relat Res*. 1993;(291):20–28.
6. Cholewicki J, McGill SM, Norman RW. Comparison of muscle forces and joint load from an optimization and EMG assisted lumbar spine model: towards development of a hybrid approach. *J Biomech*. 1995;28(3):321–331. PubMed ID: 7730390 doi:10.1016/0021-9290(94)00065-C
7. Nikooyan AA, Veeger HEJ, Westerhoff P, Graichen F, Bergmann G, van der Helm FCT. Validation of the delft shoulder and elbow model using in-vivo glenohumeral joint contact forces. *J Biomech*. 2010;43(15):3007–3014. PubMed ID: 20655049 doi:10.1016/j.jbiomech.2010.06.015
8. Nikooyan AA, Veeger HEJ, Westerhoff P, et al. An EMG-driven musculoskeletal model of the shoulder. *Hum Mov Sci*. 2012;31(2):429–447. PubMed ID: 22244106 doi:10.1016/j.humov.2011.08.006
9. Blache Y, Begon M, Michaud B, Desmoulins L, Allard P, Dal Maso F. Muscle function in glenohumeral joint stability during lifting task. *PLoS One*. 2017;12(12):e0189406. PubMed ID: 29244838 doi:10.1371/journal.pone.0189406
10. Quental C, Folgado J, Ambrósio J, Monteiro J. A new shoulder model with a biologically inspired glenohumeral joint. *Med Eng Phys*. 2016;38(9):969–977. PubMed ID: 27381499 doi:10.1016/j.medengphy.2016.06.012
11. Halder AM, Kuhl SG, Zobitz ME, Larson D, An KN. Effects of the glenoid labrum and glenohumeral abduction on stability of the shoulder joint through concavity-compression: an in vitro study. *J Bone Joint Surg Am*. 2001;83-A(7):1062–1069. doi:10.2106/00004623-200107000-00013
12. Lippitt SB, Vanderhooft JE, Harris SL, Sidles JA, Harryman DT, Matsen FA. Glenohumeral stability from concavity-compression: a quantitative analysis. *J Shoulder Elbow Surg*. 1993;2(1):27–35. PubMed ID: 22959294 doi:10.1016/S1058-2746(09)80134-1
13. van der Helm F. A finite element musculoskeletal model of the shoulder mechanism. *J Biomech*. 1994;27(5):551–569. PubMed ID: 8027090 doi:10.1016/0021-9290(94)90065-5
14. Delp SL, Anderson FC, Arnold AS, et al. OpenSim: open-source software to create and analyze dynamic simulations of movement. *IEEE Trans Biomed Eng*. 2007;54(11):1940–1950. PubMed ID: 18018689 doi:10.1109/TBME.2007.901024
15. Saul KR, Hu X, Goehler CM, et al. Benchmarking of dynamic simulation predictions in two software platforms using an upper limb musculoskeletal model. *Comput Methods Biomech Biomed Engin*. 2015;18(13):1445–1458. PubMed ID: 24995410 doi:10.1080/10255842.2014.916698

16. Wu G, van der Helm FC, Veeger HE, et al. ISB recommendation on definitions of joint coordinate systems of various joints for the reporting of human joint motion—Part II: Shoulder, elbow, wrist and hand. *J Biomech*. 2005;38(5):981–992. PubMed ID: 15844264 doi:10.1016/j.jbiomech.2004.05.042
17. de Groot JH, Brand R. A three-dimensional regression model of the shoulder rhythm. *Clin Biomech*. 2001;16(9):735–743. doi:10.1016/S0268-0033(01)00065-1
18. Millard M, Uchida T, Seth A, Delp SL. Flexing computational muscle: modeling and simulation of musculotendon dynamics. *J Biomech Eng*. 2013;135(2):021005. PubMed ID: 23445050 doi:10.1115/1.4023390
19. Binder-Markey BI, Murray WM. Incorporating the length-dependent passive-force generating muscle properties of the extrinsic finger muscles into a wrist and finger biomechanical musculoskeletal model. *J Biomech*. 2017;61:250–257. PubMed ID: 28774467 doi:10.1016/j.jbiomech.2017.06.026
20. Thelen DG, Anderson FC, Delp SL. Generating dynamic simulations of movement using computed muscle control. *J Biomech*. 2003;36(3):321–328. PubMed ID: 12594980 doi:10.1016/S0021-9290(02)00432-3
21. Thelen DG, Anderson FC. Using computed muscle control to generate forward dynamic simulations of human walking from experimental data. *J Biomech*. 2006;39(6):1107–1115. PubMed ID: 16023125 doi:10.1016/j.jbiomech.2005.02.010
22. Steele KM, Demers MS, Schwartz MH, Delp SL. Compressive tibiofemoral force during crouch gait. *Gait Posture*. 2012;35(4):556–560. PubMed ID: 22206783 doi:10.1016/j.gaitpost.2011.11.023
23. Vidt ME, Santago AC, Marsh AP, et al. The effects of a rotator cuff tear on activities of daily living in older adults: a kinematic analysis. *J Biomech*. 2016;49(4):611–617. PubMed ID: 26879327 doi:10.1016/j.jbiomech.2016.01.029
24. Cram JR, Criswell E. *Cram's Introduction to Surface Electromyography*. Sudbury, MA: Jones and Bartlett; 2011. http://www2.lib.ncsu.edu/catalog/record/NCSU2723443
25. Meszaros KA, Vidt ME, Dickerson CR. The effects of hand force variation on shoulder muscle activation during submaximal exertions. *Int J Occup Saf Ergon*. 2018;24(1):100–110. PubMed ID: 28007019 doi:10.1080/10803548.2016.1266805
26. Dal Maso F, Begon M, Raison M. Methodology to customize maximal isometric forces for hill-type muscle models. *J Appl Biomech*. 2017;33(1):80–86. PubMed ID: 27735222 doi:10.1123/jab.2016-0062
27. Pataky TC. One-dimensional statistical parametric mapping in python. *Comput Methods Biomech Biomed Engin*. 2012;15(3):295–301. PubMed ID: 21756121 doi:10.1080/10255842.2010.527837
28. Pataky TC, Robinson MA, Vanrenterghem J. Vector field statistical analysis of kinematic and force trajectories. *J Biomech*. 2013;46(14):2394–2401. PubMed ID: 23948374 doi:10.1016/j.jbiomech.2013.07.031
29. Hicks JL, Uchida TK, Seth A, Rajagopal A, Delp SL. Is my model good enough? best practices for verification and validation of musculoskeletal models and simulations of movement. *J Biomech Eng*. 2015;137(2):020905. PubMed ID: 25474098 doi:10.1115/1.4029304
30. Heuberer P, Kranzl A, Laky B, Anderl W, Wurnig C. Electromyographic analysis: shoulder muscle activity revisited. *Arch Orthop Trauma Surg*. 2015;135(4):549–563. PubMed ID: 25720847 doi:10.1007/s00402-015-2180-3
31. Wickham J, Pizzari T, Stansfeld K, Burnside A, Watson L. Quantifying "normal" shoulder muscle activity during abduction. *J Electromyogr Kinesiol*. 2010;20(2):212–222. PubMed ID: 19625195 doi:10.1016/j.jelekin.2009.06.004
32. Westerhoff P, Graichen F, Bender A, et al. In vivo measurement of shoulder joint loads during activities of daily living. *J Biomech*. 2009;42(12):1840–1849. PubMed ID: 19643418 doi:10.1016/j.jbiomech.2009.05.035
33. Westerhoff P, Graichen F, Bender A, et al. In vivo measurement of shoulder joint loads during walking with crutches. *Clin Biomech*. 2012;27(7):711–718. doi:10.1016/j.clinbiomech.2012.03.004
34. Bergmann G, Graichen F, Bender A, et al. In vivo gleno-humeral joint loads during forward flexion and abduction. *J Biomech*. 2011;44(8):1543–1552. PubMed ID: 21481879 doi:10.1016/j.jbiomech.2011.02.142
35. Bergmann G, Graichen F, Bender A, Kääb M, Rohlmann A, Westerhoff P. In vivo glenohumeral contact forces—Measurements in the first patient 7 months postoperatively. *J Biomech*. 2007;40(10):2139–2149. PubMed ID: 17169364 doi:10.1016/j.jbiomech.2006.10.037
36. Clarys JP, Massez C, Van Den Broeck M, Piette G, Robeaux R. Total telemetric surface of the front crawl. In Matsui H, Kobayashi K, eds. *Biomechanics VIII-B. International Series on Biomechanics*. Vol. 4. Chicago, IL: Human Kinetics; 1983: 951–958.
37. Hautier CA, Arsac LM, Deghdegh K, Souquet J, Belli A, Lacour JR. Influence of fatigue on EMG/force ratio and cocontraction in cycling. *Med Sci Sports Exerc*. 2000;32(4):839–843. PubMed ID: 10776904.
38. Jobe FW, Moynes DR, Tibone JE, Perry J. An EMG analysis of the shoulder in pitching: a second report. *Am J Sports Med*. 1984;12(3):218–220. PubMed ID: 6742305 doi:10.1177/036354658401200310
39. Magermans DJ, Chadwick EKJ, Veeger HEJ, Rozing PM, van der Helm FCT. Effectiveness of tendon transfers for massive rotator cuff tears: a simulation study. *Clinical Biomechanics*. 2004;19(2):116–122. PubMed ID: 14967573 doi:10.1016/j.clinbiomech.2003.09.008
40. Steenbrink F, de Groot JH, Veeger HE, van der Helm F C, Rozing PM. Glenohumeral stability in simulated rotator cuff tears. *J Biomech*. 2009;42(11):1740–1745. PubMed ID: 19450803 doi:10.1016/j.jbiomech.2009.04.011
41. van Drongelen S, Schlussel M, Arnet U, Veeger D. The influence of simulated rotator cuff tears on the risk for impingement in handbike and handrim wheelchair propulsion. *Clin Biomech*. 2013;28(5):495–501. doi:10.1016/j.clinbiomech.2013.04.007
42. Quental C, Folgado J, Ambrosio J, Monteiro J. Critical analysis of musculoskeletal modelling complexity in multibody biomechanical models of the upper limb. *Comput Methods Biomech Biomed Engin*. 2015;18(7):749–759. PubMed ID: 24156405 doi:10.1080/10255842.2013.845879